Diffusions of nanoparticles and existence of multiple solutions for MHD Williamson nanofluid with slip mechanism

Aamir Hamid[a,*] , Taseer Muhammad[b] and Muhammad Irfan[c,*]

[a]Department of Mathematics, Women University of Azad Jammu and Kashmir, Bagh 12500, Azad Kashmir, Pakistan

[b]Department of Mathematics, College of Science, King Khalid University, Abha 61413, Saudi Arabia

[c]Department of Mathematical Sciences Federal Urdu University of Arts Science and Technology, 44000, Islamabad, Pakistan

[*] (Corresponding author: **mirfan@math.qau.edu.pk (M. Irfan))**

ahamid@itu.edu.tr (Aamir Hamid)

Abstract: Here the concept of heat transport mechanisms and stagnation point of the MHD Williamson nanofluid have been elaborated with Brownian motion and thermophoresis diffusion past a permeable stretching/shrinking cylinder. Both the conditions of velocity slip and heat source/sink effects are considered. The shooting algorithm with Runge-Kutta-Fehlberg method has been exploited for solutions of ODEs. The effect on drag coefficient, heat and mass transport rates as well as the dimensionless velocity, temperature and concentration fields of the physical boundaries objectives of the study are graphically delineated and thoroughly discussed. As nanoparticle concentration increases at the outer surface of the boundary layer, the rising patterns of Nusselt number as well as skin friction are observed. Dual solutions with the critical value of the mass transfer parameter $(0 < s_c < s)$ and the shrinking parameter $(\chi_c < \chi)$ are obtained for different related parameters in some domains and shrinking parameter. Here the outcomes noted the average increase of skin friction with respect to γ (curvature) factor to 24.8% with brilliant results compared with former prose. Additionally, 6.37% and 3.46% average increase of skin friction for first solution; however, for second solution 4.98% and 3.51% enhancement noted respectively, when $\alpha = \gamma = 0$ and 0.1 with respect to χ.

Keywords: Critical values; Stagnation-point flow; Heat generation/absorption; Multiple solutions; Magneto-Williamson fluid; Shrinking cylinder.

1. Introduction

The heat transport phenomenon is discussed excessively in terms of the seven slip parameter of Buongiorno's model. The seven slip parameters involve inertial forces, Brownian diffusion, thermophoretic force, Magnus effect, fluid drainage and gravity. But in Buongiorno's model only two of them are discussed, which are Brownian motion and thermophoresis diffusion. Thermophoresis is the averaged Brownian motion of particles in a fluid that is subjected to a constant temperature gradient. The stronger molecular impulses in the hotter fluid zone move particles towards the colder fluid region, where the molecular impulses are weaker, over lengthy periods of time [1]. Further, the term thermophoresis refers to the averaged mobility of the particles. The phenomena of thermophoresis were initially observed by Tyndall in a dust-filled room when he noticed that aerosol particles were pushed away from a heated surface, but it was not researched in depth until the twentieth century [2]. Tyndall made no connection between thermophoresis and particle molecular impulses.

Electronic system cooling is a vital industrial need in today's fast-paced technological environment. The major restriction is the low thermal conductivity of widely used heat transport fluids; for instance oil, water and ethylene glycol. This necessitates the development of novel techniques capable of overcoming this constraint. Solid particles of nanoscale size (1-100 nm) have shown to be successful when suspended in conventional heat transfer fluids in the pursuit of the same task. The use of the particles has drawn great attention in the industrial application because of their miraculous property of changing the thermophysical properties of host fluid, thereby enhancing the heat transfer considerably. In 1995 at the Argonne National Laboratory, such colloidal suspension was given the name as `nanofluid' by Choi [3]. The modern development regarding the heat transfer using nanofluids and their mathematical modeling [4] have contributed immensely to the output of various industries. These fluids find wide applications in, but not limited to, biomedicine, transportation (engine cooling/vehicle thermal management), nuclear systems cooling, manufacturing, heat exchanger, and cooling of electronics. The free convective nanofluid flow along a vertical sheet was discussed by Kuznetsov and Nield [5]. They disclose

that the heat transfer rate is a diminishing function of parameters like buoyancy ratio, Brownian motion and thermophoresis parameter. Likewise, Khan and Pop [6] considered the model of Brownian diffusion and thermophoresis to investigate the boundary layer flow along a stretched surface which has constant surface temperature. They determined that the thermal transport rate is a decaying function of each dimensionless number. Ibrahim and Shanker [7] found the numerical solution and heat transport of nanofluids with convective conditions influenced by a vertical plate. Numerous studies on heat transport and nanofluid have been elaborated in Refs [8-16].

The investigation of liquid stream and heat transfer over a stretching/shrinking cylinder have increased eminent enthusiasm among the different specialists because of the quickly developing applications in numerous modern and building processes. In 1975, the fluid flow due to the stretching cylinder was described by Crane [17] and for the very first time Wang [18] investigated the fluid flow over a hollow cylinder when the surrounding liquid is very still. Lok and Pop [19] talked about the highlights of heat transfer properties over a permeable shrinking cylinder and derived the triple solutions of the problem. Further, Mukhopadhyay [20] investigated the behavior of mixed convective flow past a stretching cylinder within the sight of porosity. The attributes of heat transport of transient flow of nanofluid towards a contracting cylinder is studied by Zaimi *et al*. [21]. Ishak and Nazar [22] noticed that the local similar solution can be achieved by the stretching cylinder linearly in the axial direction. Fang *et al*. [23] obtained the exact solutions of unsteady fluid flow due to the contraction and expansion of cylinder. The results of axi-symmetric flow over a shrinking cylinder with buoyancy assisting flow were also investigated by Lok et al. [24]. Again, Zaimi *et al*. [25] utilizing a shooting scheme to get the multiple solutions of time dependent viscous fluid along a shrinking cylinder. They found that the friction factor reduces with the increment of unsteadiness parameter. The features of heat transport with impacts of velocity slip on the unsteady flow have been investigated by Abbas *et al*. [26]. Dhani *et al*. [27] have investigated the dual solutions due to an inclined stretching/shrinking cylinder in the presence of nanoparticles. They introduced the mathematical investigation of blended convection stream and warmth move examination within the sight of joint impacts Brownian movement, thermophoresis, and Joule dissemination. They have seen that warmth move rate increments with pull boundary; however, shows an inverse example with warm slip boundary. The impacts of entropy improvement of a gooey liquid past a hyperbolic chamber are broken down by Majeed et al. [28]. As of late, the liquid stream and warmth move studies with numerous physical perspectives are

proposed by [29,30].

Furthermore, the attention of researchers and experts to study the arena of nanofluid is better than formerly caused by immense uses of nanofluid in the engineering, bio-sciences and modern technology. Here the study focused on impacts of magnetic field [31-38], stagnation flow and mass suction parameter for unsteady Williamson [39-41] nanofluid influenced by stretching/shrinking cylinder. Here also pointed out the some novelty of the present research problem which have been reported as; utilization of MHD have mechanical and industrial usages, comprising inventors and electrical filters, reactor icy, hydro-magnetic antenna, magnetic pills targeting, control forces, and so on. The presence of nanofluid i.e., the recent progresses in industrial and scientific equipment have made several phenomena that were formerly doubtful feasible because of the growth of nanoparticles conceivable. Therefore, melting a solid metal element in thermal transmitting liquid can remarkably increase the heat conductivity of fluid. In the entire article the present theory provides several supports in the informatics arena of sciences, i.e., pharmacological science and machinery areas for instance interstellar equipment, atomic vessel chilling, heat and lightening procedure, and various others. The theory of heat sink/source has a key role in the omission of heat from the debris of atomic energy, shed discarded radioactive material, radiating diffusers, preservation of metal pieces, and rough grease recovery. Furthermore, the several unique/multiple solutions for dimensionless velocity/temperature/concentration profiles and skin friction coefficients/Nusselt number/Sherwood number using local-similarity transformation. The comparative analyses via tables are also presented.

2. Modeling

Here we considered two-dimensional, axisymmetric, unsteady, incompressible MHD flow of Williamson nanofluid via stretching cylinder. The properties of heat source/sink and slip condition on velocity are also investigated in this study. The flow is driven by a permeable infinite cylinder of radius R. The physical model that we have obtained is illustrated in **Fig. 1**. The cylinder is stretching with velocity $u_w(x,t)=\frac{ax}{1-\beta t}$, while $u_e(x,t)=\frac{bx}{1-\beta t}$ the free stream velocity. A strength $B=(0,B_0,0)$ non-uniform transverse magnetic field, where B_0 is the constant applied magnetic field.

The mathematical form of Williamson model is expressed as $\mu = \mu_\infty + \left(\mu_0 - \mu_\infty\right)\left(1 - \Gamma\dot{\gamma}\right)^{-1}$.

Therefore, above assumptions and the standard estimates of boundary layer report the following equations [42-44]:

2.1.Continuity:

$$\frac{\partial(ru)}{\partial x} + \frac{\partial(rv)}{\partial r} = 0, \tag{1}$$

2.2.Momentum equation:

$$\frac{\partial u}{\partial t} + u\frac{\partial u}{\partial x} + v\frac{\partial u}{\partial r} = \frac{\nu}{r}\frac{\partial u}{\partial r}\left[\beta^* + \left(1-\beta^*\right)\left(1-\Gamma\frac{\partial u}{\partial r}\right)^{-1}\right] + \nu\Gamma\frac{\partial u}{\partial r}\frac{\partial^2 u}{\partial r^2}\left[\left(1-\beta^*\right)\left(1-\Gamma\frac{\partial u}{\partial r}\right)^{-2}\right]\frac{\partial u}{\partial t} + u\frac{\partial u}{\partial x} + v\frac{\partial u}{\partial r} = \frac{\nu}{r}\frac{\partial u}{\partial r}\left[\beta^* + \left(1-\beta^*\right)\left(1-\Gamma\frac{\partial u}{\partial r}\right)^{-1}\right]$$

$$+\nu\Gamma\frac{\partial u}{\partial r}\frac{\partial^2 u}{\partial r^2}\left[\left(1-\beta^*\right)\left(1-\Gamma\frac{\partial u}{\partial r}\right)^{-2}\right] + \nu\frac{\partial^2 u}{\partial r^2}\left[\beta^* + \left(1-\beta^*\right)\left(1-\Gamma\frac{\partial u}{\partial r}\right)^{-1}\right] + \frac{\partial U_e}{\partial t} + U_e\frac{\partial U_e}{\partial x} - \frac{\sigma B^2(t)}{\rho}\left(u - U_e\right),$$

(2)

2.3.Energy equation:

$$\frac{\partial T}{\partial t} + u\frac{\partial T}{\partial x} + v\frac{\partial T}{\partial r} = \frac{k}{\rho c_p}\left(\frac{\partial^2 T}{\partial r^2} + \frac{1}{r}\frac{\partial T}{\partial r}\right) + \tau\left[D_B\frac{\partial C}{\partial r}\frac{\partial T}{\partial r} + \frac{D_T}{T_\infty}\left(\frac{\partial T}{\partial r}\right)^2\right] + \frac{Q_0}{(\rho c)_f}\left(T - T_\infty\right), \tag{3}$$

2.4.Concentration equation:

$$\frac{\partial C}{\partial t} + u\frac{\partial C}{\partial x} + v\frac{\partial C}{\partial r} = \frac{D_B}{r}\frac{\partial}{\partial r}\left(r\frac{\partial C}{\partial r}\right) + \frac{D_T}{T_\infty}\frac{1}{r}\frac{\partial}{\partial r}\left(r\frac{\partial T}{\partial r}\right). \tag{4}$$

with the allied boundary conditions we have:

$$u = u_w(x,t) + u_{slip}, \quad v = v_w, \quad T = T_w, \quad C = C_w \quad at \quad r = R \tag{5}$$

$$u \to u_e, \qquad T \to T_\infty, \qquad C \to C_\infty \quad r \to \infty. \tag{6}$$

2.5.Similarity solution of unsteady flow

To solve the governing equations (2)-(6), the following dimensionless variables are introduced:

$$\eta = \frac{r^2 - R^2}{2R}\left(\frac{u_w}{\nu x}\right)^{1/2}, \quad \psi = \left(u_w \nu x\right)^{1/2} Rf(\eta), \quad \theta(\eta) = \frac{T - T_\infty}{T_w - T_\infty}, \quad \varphi(\eta) = \frac{C - C_\infty}{C_w - C_\infty}. \tag{7}$$

Eq. (1) is fulfilled automatically by using the Eq. (7) and Eqs. (2), (3) and (4) become:

$$(1+2\gamma\eta)\left[\beta^{*}+(1-\beta^{*})(1-Wef'')^{-2}\right]f'''+ff''+1-A\left(f'+\frac{\eta}{2}f''+1\right)$$
$$-M^{2}(f'-1)+2\gamma f''\left[\beta^{*}+(1-\beta^{*})\left(1-\frac{Wef''}{2}\right)(1-Wef'')^{-2}\right]=0, \tag{8}$$

$$(1+2\gamma\eta)\theta+2\gamma\theta'+Prf\theta'+Pr(1+2\gamma\eta)\left(N_b\theta'\varphi'+N_t\theta'^{2}\right)-PrA\frac{\eta}{2}\theta'+Pr\delta\theta=0, \tag{9}$$

$$(1+2\gamma\eta)\varphi''+2\gamma\varphi'+Scf\varphi'+\frac{N_t}{N_b}\left[(1+2\gamma\eta)\theta''+2\gamma\theta'\right]-ScA\frac{\eta}{2}\varphi'=0, \tag{10}$$

and transformed boundary conditions are:

$$f(0)=s,\quad f'(0)=\chi+\alpha f''\left[\beta^{*}+(1-\beta^{*})(1-Wef'')^{-1}\right],\quad \theta(0)=1,\quad \varphi(0)=1, \tag{11}$$

$$f'(\infty)\to 1,\quad \theta(\infty)\to 0,\quad \varphi(\infty)\to 0. \tag{12}$$

Here, the local Weissenberg number, the curvature parameter, the heat generation/absorption parameter, the velocity slip parameter, the magnetic parameter, the thermophoresis parameter, the Brownian motion parameter, the Prandtl number, the Schmidt number, the unsteadiness parameter, the ratio of viscosities respectively are

$$We=\left(\frac{a^{3}x^{2}r^{2}\Gamma^{2}}{(1-\beta t)^{3}R^{2}\nu}\right)^{1/2},\gamma=\left(\frac{\nu(1-\beta t)}{aR^{2}}\right)^{1/2},\delta=\left(\frac{Q_0(1-\beta t)}{a(\rho c)_f}\right),\alpha=\left(L\sqrt{\frac{a}{\nu}}\right)$$
$$M=\left(\frac{\sigma B_0^{2}}{\rho a}\right)^{1/2},N_t=\left(\frac{\tau D_B(T_w-T_\infty)}{\nu T_\infty}\right),N_b=\left(\frac{\tau D_B(C_w-C_\infty)}{\nu}\right),\Pr=\left(\frac{\mu c_p}{k}\right) \tag{13}$$
$$Sc=\left(\frac{\nu}{D_B}\right),A=\left(\frac{c}{a}\right),\beta^{*}=\left(\frac{\mu_\infty}{\mu_0}\right)$$

and $\chi>0$ for stretching cylinder and $\chi<0$ for shrinking cylinder.

3. Physical quantities

The skin friction and thermo-solutal transport are depicted as:

$$C_f=\frac{\tau_{rx}\big|_{r=R}}{\rho U^{2}},\quad Nu=\frac{xq_w\big|_{r=R}}{k(T_f-T_\infty)},\quad Sh=\frac{xq_m\big|_{r=R}}{D(C_f-C_\infty)}, \tag{14}$$

where τ_{rx}, q_w and q_m are written as:

$$\tau_{rx}=\mu_0\frac{\partial u}{\partial r}\left[\beta^{*}+(1-\beta^{*})\left(1-\Gamma\frac{\partial u}{\partial r}\right)\right],\quad q_w=-k\left(\frac{\partial T}{\partial r}\right),\quad q_m=-D\left(\frac{\partial C}{\partial r}\right). \tag{15}$$

Using (7), (14) and (15) we get

$$\mathrm{Re}^{\frac{1}{2}} C_f = f''(0)\left[\beta^* + (1-\beta^*)(1-Wef''(0))^{-1}\right],\ \mathrm{Re}^{-\frac{1}{2}} Nu = -\theta'(0),\ \mathrm{Re}^{-\frac{1}{2}} Sh = -\varphi'(0), \qquad (16)$$

where $\mathrm{Re} = xU_w / \nu$ display the local Reynolds number.

4. Solution process

Here Eqs.(8)-(10) along boundary conditions (11 and 12) have been tackled numerically through shooting scheme with RK method. The final system is reduced ODEs, which is then converted into an initial value problem, as follows:

$$f = X_1, f' = X_2, f'' = X_3, \theta = X_4, \theta' = X_5, \varphi = X_6, \varphi' = X_7. \qquad (17)$$

10^{-6} (18)

and analogous initial conditions:

$$\begin{pmatrix} X_1(0) \\ X_2(0) \\ X_2(\infty) \\ X_4(0) \\ X_4(\infty) \\ X_6(0) \\ X_6(\infty) \end{pmatrix} = \begin{pmatrix} s \\ \chi + \alpha X_3\left[\beta^* + (1-\beta^*)(1-WeX_3)^{-1}\right] \\ 1 \\ 1 \\ 0 \\ 1 \\ 0 \end{pmatrix}. \qquad (18)$$

To solve the Eq. (18) as an initial value problem, we require seven initial conditions in which four initial conditions are known while the three initial conditions X_3, X_5 and X_6 i-e., $f''(0)$, $\theta'(0)$ and $\varphi(0)$ are unknown. Hence, it is important to select the proper value of these unknowns to such an extent that far field conditions with the reasonable area length η_∞. The step size is set to $h = 0.01$ and the method is reiterated up until the acquired results converge to the preferred level of accurateness which is 10^{-6}.

4.1. Code verification

To show the precision and legitimacy of our mathematical methodology, we did an examination between the got outcomes and those distributed before by Mat *et al*. [45], Hashim and Khan [30]

and Omar *et al*. [46]. In **Table 1** , the results for reduced skin friction $\mathrm{Re}^{1/2} C_f$ are compared with those obtained by Mat *et al*. [45] and Hashim and Khan [30], who examined the slip-flow past a shrinking/stretching cylinder. In **Table 2**, the consequences of are approved against the distributed work [30] for varying γ in some special cases of Newtonian flow. Henceforth, it tends to be cultivated that our computational code utilizing Runge-Kutta-Fehlberg strategy with shooting procedure envisions accurately the liquid stream.

5. Analysis

Here our main focus is to comprehend the physical critical of the numerical model by means of graphical structures. The influences of unsteadiness parameter A magnetic parameter M local Weissenberg number We, curvature parameter γ, heat generation/absorption parameter δ velocity slip parameter α, viscosity ratio parameter β^*, shrinking parameter χ, suction parameter s have graphically scrutinized. We have fixed default values for controlling parameters as $\chi = -2.0,\ A = 0.03, M = 0.2 \beta^* = \alpha = \delta = N_t = N_b = \gamma = 0.1, We = \mathrm{Pr} = Sc = 1.0$ and $s = 1.3$ all through the calculations, in any case referenced. Additionally, the current article report the ranges of physical parameters i.e., $0 \le A \le 0.05,\ 0.8 \le We \le 1.2,\ 0.1 \le \beta^* \le 0.5,\ 0.3 \le \gamma \le 0.5,$ $0.1 \le \alpha \le 0.5,\ 0 \le M \le 0.2,\ 0 \le \delta \le 0.1$ for graphical pictures. Furthermore, the tabular comparison are made by the following ranges of parameters $0.1 \le \alpha \le 0.2,\ -1.2 \le \chi \le 2,$ $0 \le \gamma \le 0.4$ with outstanding outcomes. The variation of dimensionless skin friction $\mathrm{Re}^{1/2} C_f$, local Nusselt number $\mathrm{Re}^{-1/2} Nu$, local Sherwood number $\mathrm{Re}^{-1/2} Sh$, velocity $f'(\eta)$, temperature $\theta(\eta)$ and nanoparticle concentration $\varphi(\eta)$ are designed, where solid lines signify the upper branch (first) solution, whereas the lower branch (second) solution is spoken to by sketched lines. Furthermore, for the best and accurate results we varying the values for specific graph by fixed other parametric values fix because it's will give better convergence.

Fig. 2 *and* 3 unveil the impact of unsteadiness parameter A on $\mathrm{Re}^{\frac{1}{2}} C_f$ and $\mathrm{Re}^{-\frac{1}{2}} Nu$ against the shrinking parameter χ. These plots range of existence of both solutions are $\chi_c = (-2.1170, -2.0666, -2.0352) \le \chi \le -1.2$ when $A = 0.0, 0.03$ and 0.05. The critical values shows that the second solution shrinks for larger A in existence domain. The both upper branch

solutions of $\mathrm{Re}^{\frac{1}{2}} C_f$ and $\mathrm{Re}^{-\frac{1}{2}} Nu$ depicts the decreasing performance for larger A whereas, a opposite form is depicted for lower branch solution of $\mathrm{Re}^{\frac{1}{2}} C_f$ and $\mathrm{Re}^{-\frac{1}{2}} Nu$.

The variation of $f''(0)\left[\beta^* + (1-\beta^*)(1-Wef''(0))^{-1}\right]$ and $-\theta'(0)$ with mass transfer parameter s for representative values of We are delineated in **Fig.** 4 and 5. These plots deliver that the dual solutions $\mathrm{Re}^{\frac{1}{2}} C_f$ and $\mathrm{Re}^{-\frac{1}{2}} Nu$ are influenced by s keeping other parameters fixed. These figures reports that the dual nature of the solutions happens for the specific value of local Weissenberg number $We = 0.8, 1.0$ and 1.2. The critical value of suction parameter $s_c = (1.2227, 1.1781, 1.0119)$ as We changes from 0.8 to 1.2 We perceive that the first solution of both $\mathrm{Re}^{\frac{1}{2}} C_f$ and $\mathrm{Re}^{-\frac{1}{2}} Nu$ at the surface increase by higher values of Weissenberg number. While, $f''(0)\left[\beta^* + (1-\beta^*)(1-Wef''(0))^{-1}\right]$ and $-\theta'(0)$ shows a declining design with higher We at the boundary for second solution.

Figs. 6, 7 and 8 show the effect of viscosity ratio parameter β^* on $\mathrm{Re}^{\frac{1}{2}} C_f$, $\mathrm{Re}^{-\frac{1}{2}} Nu$ and $\mathrm{Re}^{-\frac{1}{2}} Sh$ at the surface of the cylinder, respectively. The critical value of shrinking parameter χ_c is noted for each estimation of viscosity ratio parameter, which reduces from -2.0666 to -2.1598 as χ increases from -2.5 to -1.2. It is also found that first solution is consistently greater than second solution. The first solution of $\mathrm{Re}^{\frac{1}{2}} C_f$, $\mathrm{Re}^{-\frac{1}{2}} Nu$ and $\mathrm{Re}^{-\frac{1}{2}} Sh$ increase for growing β^*. While if there should arise an occurrence of lower solution (second solution), the $f''(0)\left[\beta^* + (1-\beta^*)(1-Wef''(0))^{-1}\right]$ diminishes and invert pattern is found for $-\theta'(0)$ and $-\varphi'(0)$.

The trajectories of skin friction $\mathrm{Re}^{\frac{1}{2}} C_f$, local Nusselt number $-\theta'(0)$ and local Sherwood number $-\varphi'(0)$ for varying curvature parameter γ are depicted in **Figs.** 9, 10 and 11 against mass transfer parameter s. The dual behavior of the $\mathrm{Re}^{\frac{1}{2}} C_f$, $\mathrm{Re}^{-\frac{1}{2}} Nu$ and $\mathrm{Re}^{-\frac{1}{2}} Sh$ has been

accounted for $\gamma = 0.3, 0.4, 0.5$. The critical values of mass transfer parameter (s_c) changes from 0.1273 to -0.6526, as s changes from -0.8 to 0.8. As per these figures, we see that $|s_c|$ increments as γ improved, consequently rising the curvature parameter γ augment the range of s for which a dual solution exists. The outcomes appeared in these plots show that as γ increases the first solution of $f''(0)\left[\beta^* + (1-\beta^*)(1-Wef''(0))^{-1}\right]$, $-\theta'(0)$ and $-\varphi'(0)$ also increases. In case of second solution, skin friction coefficient $\mathrm{Re}^{\frac{1}{2}} C_f$ and rate of heat transfer $-\theta'(0)$ delineates a diminishing conduct while an expanding pattern is seen for rate of mass transfer $-\varphi'(0)$.

Fig. 12 disclose the effects of slip parameter on local Nusselt number $-\theta'(0)$. The critical values of s_c corresponding to different slip parameter are listed in this plot. The existence range of dual solution is $s_c = (-0.4125, 0.1537, 1.1781) \le s \le 2.0$ when $\alpha = 0.1, 0.3$ and 0.5. The higher values of α the second solution diminishes. Furthermore, the solution of upper branch the $\mathrm{Re}^{-\frac{1}{2}} Nu$ depicts the increasing drift while the lower one shows the decreasing pattern.

Fig. 13 is portrayed for the dual velocity profile $f'(\eta)$ for some specific value of the $(\chi = -2.0)$ with unsteadiness parameter A. The dual nature of solution for velocity profile illustrates that for growing values of A have reverse drift for both solutions. It is said that physically the first solution is stable and feasible; however, the other solution is unstable.

Currently, we will consider how the attractive parameter M affects $f'(\eta)$ and $\theta(\eta)$. The effect of M on $f'(\eta)$ and $\theta(\eta)$ is demonstrated in **Figs.** 14 and 15. The **Fig**. 14 shows that in shrinking cylinder situation, the point velocity enriches the first solution with an increase of M and the second solution with a decrease. Physically, this is the product of the decelerating effect on the flow of the drag force resulting from the applied magnetic field for a nanofluid. **Fig**. 15 indicates that the fluid temperature at the point decreased with increasing in M, except for the small section near the upper solution surface and causes changes in the magnetic parameter M for the lower solution. From a physical perspective, with an increase in M, the range of opposite cellular flow above the cylinder surface decreases, and $\theta(\eta)$. is therefore influenced by the advection of the

liquid velocity exceeding the cylinder. Further, noted that thermal thickness is greater in the situation of the upper solution as compared to the lower solution.

Next, our goal is to represent the multiple highlights for the velocity $f'(\eta)$ and temperature profiles $\theta(\eta)$ for estimations of viscosity ratio parameter β^* through **Figs.** 16 and 17. From these figures, it is revealed that both solutions for velocity field increases by rising of β^* whereas an opposite behavior is exhibited for $\theta(\eta)$. We further observed that the boundary thickness of the first solution is slenderer as compared to second solution.

Figs. 18 and 19 show the effect of heat generation parameter $(\delta > 0)$ and velocity slip parameter α on temperature distribution $\theta(\eta)$. It is seen from the **Fig.** 18 both first and second solutions for temperature profile amplify with the expansion in heat generation parameter δ. Furthermore, as can be seen, the temperature profile rises as the heat generation parameter rises. This is due to the fact that heat generation behaves as a heat sink, increasing the dimensionless temperature directly. Furthermore, we can detect from heat generation parameter mathematical expression that in case of heat generation heat is delivered to the fluid because of which temperature field of Williamson fluid growths. **Fig**. 19 displays that for a shrinking cylinder, the temperature at a point has reverse performance as α enlarges for both solutions except in a small portion close to the cylinder. Because velocity slip parameter primarily slows the fluid motion, it effectively confirms a decrease in the net flow of fluid molecules. As a result, temperature profile is reduced due to less molecule mobility. However, for first solution of $\theta(\eta)$ has lesser magnitude in assessment with lowered one.

6. Conclusions

The current research focused on the dual solutions on MHD magnetite Williamson nanofluid caused by a permeable stretching/shrinking cylinder. The stagnation flow and slip boundary condition at the surface with mass transfer parameter is numerically computed. The shooting process has been exploited for solutions. For this model, the dual nature of solutions has been identified under the influence of some specific physical parameters. The following conclusions are drawn:

- Some critical range of χ_c and s_c are found for the existence of both solutions first and second one.
- The rate of heat transfer decreases as velocity slip parameter increases.
- The rate of mass transfer at the surface increases with higher curvature parameter .
- The temperature of the nanofluid increases with increasing values of heat generation/absorption parameter.
- The average intensification of skin friction with respect to curvature factor was noted to be 24.8% with comparison of former work.
- The first and second solutions average enhancement for skin friction for shrinking parameter was examined to be 6.37% and 4.98% respectively, when velocity slip and curvature factors are absence.
- For comparative results the minimum value of $\alpha = 0.1, \chi = -1.2 \text{ and } \gamma = 0$, while maximum values of $\alpha = 0.2, \chi = 2 \text{ and } \gamma = 0.4$ explored remarkable results for skin friction coefficient for both solutions.
- Physically, first solution is efficient and stable compared with second solution.

Acknowledgement: The authors extend their appreciation to the Deanship of Research and Graduate Studies at King Khalid University, Abha, Saudi Arabia for funding this work through General Research Project under grant number GRP/67/45.

Authors credit statement

The corresponding author is responsible for ensuring that the descriptions are accurate and agreed by all authors. All authors contribute positively in the revised version of the manuscript. Some author help to improve language some help for results and discussion and also for improvement of better results.

Credit author statement

All the descriptions are accurate and agreed by all authors and contribute positively.

Declaration of Competing Interest

The author declared no conflict of interest for this submission.

References:

1. Haw, M., ‘’Einstein’s random walk’’, Phys. World, 19-22 (2005).
2. Tyndall, J., ‘’On haze and dust’’, Proc. R. Inst., 6, 1-6 (1870).
3. Choi, S.U.S., ‘’Enhancing thermal conductivity of fluids with nanoparticles’’, ASME-Publications-Fed, $231, 99-106$ (1995) .
4. Buongiorno, J., ‘’Convective transport in nanofluids’’, J. Heat Transf., $128, 240-250$ (2006) https://doi.org/10.1115/1.2150834.
5. Kuznetsov, A., and Nield, D., ‘’The Cheng-Minkowycz problem for natural convective boundary layer flow in a porous medium saturated by a nanofluid: a revised model’’, Int. J. Heat Mass Transf., $65, 682-685$ (2013) https://doi.org/10.1016/j.ijheatmasstransfer.2013.06.054.
6. Khan, W.A., and Pop, I., ‘’Boundary-layer flow of a nanofluid past a stretching sheet, Int. J. Heat Mass Transf.,’’ $53, 2477-2483$ (2010) https://doi.org/10.1016/j.ijheatmasstransfer.2010.01.032.
7. Ibrahim, W., and Shanker, B., ‘’Boundary layer flow and heat transfer of nanofluid over a vertical plate with convective surface boundary condition’’, ASME. J. Fluids Eng., 8 (2012) https://doi.org/$10.1115/1.4007075$.
8. Khan, S.U., and Khan, H.A., Swimming of gyrotactic microorganisms in unsteady flow of Eyring Powell nanofluid with variable thermal features: Some bio-technology applications, Int. J. Thermophysics, 41 (2020) https://doi.org/10.1007/s10765-023-03267-2.
9. Shah, F., Khan, S.A., K. Al-Khaled, Khan, M.I., et al., ‘’Impact of entropy optimized Darcy-Forchheimer flow in MnZnFe2O4 and NiZnFe2O4 hybrid nanofluid towards a curved surface’’, Zeitschrift für Angewandte Mathematik und Mechanik, 102, (2021) https://doi.org/10.1002/zamm.202100194.
10. Irfan, M., Anwar, M.S., Kebail, I., and Khan, W.A., ‘’Thermal study on the performance of Joule heating and Sour-Dufour influence on nonlinear mixed convection radiative flow of Carreau nanofluid’’, Tribology Int., 188, 108789 (2023) https://doi.org/10.1016/j.triboint.2023.108789.
11. Khan, W.A., Anjum, N., Hobiny A., and ALi, M., ‘’Entropy generation analysis for chemically

reactive flow of Sutterby nanofluid considering radiation aspects'', Scientia Iranica, (2023) doi:10.24200/SCI.2023.60105.6594.

12. Raza, A., Al-Khaled, K., Muhammad, T., and Khan, S.U., ''Accelerating flow of carbon nanotubes with carboxymethyl cellulose and blood base materials with comparative thermal features: Prabhakar fractional model'', Mathematical Prob. Eng., 2023, 3468295 (2023) https://doi.org/10.1155/2023/3468295.
13. Manigandan, A., and Narayana, P.V.S., ''Influence of variable thermal conductivity and mixed convection on hybrid nanofluid (SWCNT + MWCNT/H2O) flow over an exponentially elongated sheet with slip conditions'', Indian J. Phy., (2023) https://doi.org/10.1007/s12648-023-02912-8.
14. Guedri, K., Sadiq, M., Hashmi, et al., ''Numerical Simulation for Two-Phase Dusty Thermally Developed Marangoni Forced Convective Flow of Williamson Material: A Finite Difference Scheme'', Zeitschrift für Angewandte Mathematik und Mechanik, (2023), https://doi.org/10.1002/zamm.202100206.
15. Irfan, M., ''Energy transport phenomenon via Joule heating and aspects of Arrhenius activation energy in Maxwell nanofluid'', Waves Random Complex Media, (2023) https://doi.org/10.1080/17455030.2023.2196348.
16. Ahmad, H., Al-Khaled, K., Sowayan, A.S., et al., ''Experimental investigation for automotive radiator heat transfer performance with ZnO-Al2O3/water based hybird nanoparticles: An improved thermal model'', Int. J. Modern Physics B, 37, 2350050 (2023) https://doi.org/10.1142/S0217979223500509.
17. Crane, L.J., ''Boundary layer flow due to a stretching cylinder'', ZAMP, 26, 619-622 (1975) https://doi.org/10.1007/BF01594034.
18. Wang, C.Y., ''Fluid flow due to a stretching cylinder'', Phys. Fluids, 31 (1988) https://doi.org/10.1063/1.866827.
19. Lok, Y.Y., and Pop, I., ''Wang's shrinking cylinder problem with suction near a stagnation point'', Phys. Fluids, 23, 083102 (2011) https://doi.org/10.1063/1.3624697.
20. Mukhopadhyay, S., ''Mixed convection boundary layer flow along a stretching cylinder in porous medium'', J. Petroleum Sci. Eng., 96, 73-78 (2012) https://doi.org/10.1016/j.petrol.2012.08.006.
21. Zaimi, K., Ishak, A., and Pop, I., ''Unsteady flow due to a contracting cylinder in a

nanofluid using Buongiorno's model'', Int. J. Heat Mass Transf., 68, 509-513 (2014) https://doi.org/10.1016/j.ijheatmasstransfer.2013.09.047.

22. Ishak, A., and Nazar, R., ''Laminar boundary layer flow along a stretching cylinder'', Eur. J. Sci., 36, 22-29 (2009) https://doi.org /10.3844/jmssp.2014.117.124.
23. Fang, T., Zhang, J., and Zhong, Y., ''Note on unsteady viscous flow on the outside of an expanding or contracting cylinder'', Commun. Nonlinear Sci. Numer. Simulat., 17, 3124-3128 (2012) https://doi.org/10.1016/j.cnsns.2011.12.013.
24. Lok, Y.Y., Merkin, J.H., and Pop, I., ''Mixed convection flow near the axisymmetric stagnation point on a stretching or shrinking cylinder'', Int. J. Thermal Sci., 59, 186-194 (2012) https://doi.org/10.1016/j.ijthermalsci.2012.04.008.
25. Zaimi, W.M.K.A.W., Ishaq, A., and Pop, I., ''Unsteady viscous flow over a shrinking cylinder'', J. King Saud University, 25, 143-148 (2013) https://doi.org/10.1016/j.jksus.2012.11.005.
26. Abbas, Z., Rasool, S., and Rashidi, M.M., ''Heat transfer analysis due to an unsteady stretching/shrinking cylinder with partial slip condition and suction'', Ain Shams Emng. J., 6 939-945 (2015) https://doi.org/10.1016/j.asej.2015.01.004.
27. Dhanai, R., Rana, P., and Kumar, L., ''MHD mixed convection nanofluid flow and heat transfer over an inclined cylinder due to velocity and thermal slip effects: Buongiorno's model, Powd. Tech., 288, 140-150 (2016) https://doi.org/10.1016/j.powtec.2015.11.004.
28. Majeed, A., Javed, T., and Mustafa, I., ''Heat transfer analysis of boundary layer flow over hyperbolic stretching cylinder'', Alex. Eng. J., 55, 1333-1339 (2016) https://doi.org/10.1016/j.aej.2016.04.028.
29. Hamid, A., Hashim and Khan, M., ''Impacts of binary chemical reaction with activation energy on unsteady flow of magneto-Williamson nanofluid'', J. Mol. Liq., 262, 435-442 (2018) https://doi.org/10.1016/j.molliq.2018.04.095.
30. Hashim and Khan, M., ''Critical values in flow patterns of Magneto-Carreau fluid over a circular cylinder with diffusion species: Multiple solutions'', J. Taiwan Inst. Chem. Eng., 77, 282-292 (2017) https://doi.org/10.1016/j.jtice.2017.04.047.
31. Khan, M., Irfan, M., Ahmad, L., and Khan, W.A., ''Simultaneous investigation of MHD and convective phenomena on time-dependent flow of Carreau nanofluid with variable properties: Dual solutions'', Phy. Let. A, 382, 2334-2342 (2018)

https://doi.org/10.1016/j.physleta.2018.05.033.

32. Irfan, M., Khan, M., Khan, W.A., and Ahmad, L., ‘’Influence of binary chemical reaction with Arrhenius activation energy in MHD nonlinear radiative flow of unsteady Carreau nanofluid: dual solutions’’, Appl Phy. A, 125 (2019) https://doi.org/10.1007/s00339-019-2457-4.
33. Shamshuddin, M.D., Mabood, F., and Salawu, S.O., ‘’Flow of three-dimensional radiative Williamson fluid over an inclined stretching sheet with Hall current and nth-order chemical reaction’’, Heat Transf., (2021) https://doi.org/10.1002/htj.22130.
34. Humane, P.P., Patil, V.S., Patil, A.B., et al., ‘’Dynamics of multiple slip boundaries effect on MHD Casson-Williamson double-diffusive nanofluid flow past an inclined magnetic stretching sheet’’, Proceedings Ins. Mech. Eng. Part E: J. Process Mech. Eng., 236 (2022) https://doi.org/10.1177/09544089221078153.
35. Tabrez, M., Khan, W.A., Irfan, M., et al., ‘’Analysis of oxytactic microorganisms and magnetic dipole for radiative cross fluid flow configured by nano-enhanced phase materials’’, Scientia Iranica, (2023) https://doi.org/10.24200/SCI.2023.60843.7018.
36. Shamshuddin, M.D., Saeed, A., Mishra, S.R., et al., ‘’Homotopic simulation of MHD bioconvective flow of water-based hybrid nanofluid over a thermal convective exponential stretching surface’’, Int. J. Numer. Methods for Heat Fluid Flow, (2023) https://doi.org/10.1108/HFF-03-2023-0128.
37. Anwar, M.S., Muhammad, T., Khan, M., et al., ‘’MHD nanofluid flow through Darcy medium with thermal radiation and heat source’’, Int. J. Modern Phy. B, (2023) https://doi.org/10.1142/S0217979224503867.
38. Irfan, M., and Muhammad, T., ‘’Computational framework of MHD radiative heat transfer to Carreau nanofluid with Soret-Dufour effects and activation energy’’, J. Appl. Math. Mechanics, Zeitschrift für Angewandte Mathematik und Mechanik, (2023) https://doi.org/10.1002/zamm.202300410.
39. Shamshuddin, M.D., Salawu, S.O., Shahzad, F., et al., ‘’Thermal examination of chemical interaction and thermophoretic diffusion of Williamson fluid flow across Riga Plate surface with nonlinearity radiation flux’’, Numer. Heat Transf. Part A: Applications, (2023) https://doi.org/10.1080/10407782.2023.2251092.

40. Ali, U., Irfan, M., Akbar, N.S., et al., ‘’Dynamics of Soret–Dufour effects and thermal aspects of Joule heating in multiple slips Casson–Williamson nanofluid’’, Int. J. Modern Physics B, (2023) https://doi.org/10.1142/S0217979224502060.
41. Usman, Shaheen, S., Arain, M.B., et al., ‘’A case study of heat transmission in a Williamson fluid flow through a ciliated porous channel: A semi-numerical approach, Case Stud. Ther. Eng.,’’ 41 (2023) https://doi.org/10.1016/j.csite.2022.102523.
42. Hamid, A., Hashim and Khan, M., ‘’Impacts of binary chemical reaction with activation energy on unsteady flow of magneto-Williamson nanofluid’’, J. Mol. Liq., 262, 435-442 (2018) https://doi.org/10.1016/j.molliq.2018.04.095.
43. Song, Y.Q., Hamid, A., Sun, T.C., et al., ‘’Unsteady mixed convection flow of magneto-Williamson nanofluid due to stretched cylinder with significant non-uniform heat source/sink features’’, Alexandria Eng. J., 61, 195–206 (2022) https://doi.org/10.1016/j.aej.2021.04.089.
44. Khan, M., Hamid, A., and Hashim, ‘’Effects of Thermal Radiation and Slip Mechanism on Mixed Convection Flow of Williamson Nanofluid Over an Inclined Stretching Cylinder’’, Commun. Theor. Phys., 71, 1405 (2019) https://doi.org/10.1088/0253-6102/71/12/1405.
45. Mat, N.A.A., Arifin, N.M., Nazar, R., and Bachok, N., ‘’Boundary layer stagnation-point flow and heat transfer towards a shrinking/stretching cylinder over a permeable surface’’, Appl. Math., 6, 466-475 (2015) https://doi.org/10.4236/am.2015.63044.
46. Omar, N.S., Bachok, N., and Arifin, N.M., ‘’Stagnation point flow over a stretching or shrinking cylinder in a copper-water nanofluid’’, Int. J. Sci. Tech., 8 (2015) https://doi.org/10.17485/ijst/2015/v8i31/85405.

Biographies

Aamir Hamid is an Assistant professor at Women University of Azad Jamu and Kashmir, Bagh Pakistan. He received PhD degree in Mathematics in the field of Fluid Mechanics, Quaid-i-Azam University Islamabad, Pakistan. His research interests included is Fluid Mechanics and published 63 research articles appear in reputable international journals.

Taseer Muhammad is an Assistant professor at Department of Mathematics, College of Science, King Khalid University, Abha, Saudi Arabia. He received PhD in Mathematics, Quaid-I-Azam

University, Islamabad, Pakistan. His research interests included is Fluid Mechanics. His published research articles appear in reputable international journals.

Muhammad Irfan is an Assistant professor at Federal Urdu University of Arts Sciences and Technology, Islamabad, Pakistan. He received PhD degree in Mathematics in the field of Fluid Mechanics, Quaid-i-Azam University Islamabad, Pakistan. His research interests included is Fluid Mechanics and published 110 research articles appear in reputable international journals.

Nomenclature			
u, v	Velocity components	x, r	Cartesian coordinates
Γ	Relaxation time	f', θ, ϕ	Fluid concentration
ρ	Fluid density	C_w	Surface volume fraction
T	Fluid temperature	C_∞	Ambient nanoparticle volume fraction
T_w	Surface temperature	U_w	Stretching velocity
T_∞	Ambient temperature	μ_0, μ_∞	(Zero, infinite) shear viscosities
μ	Generalized Newtonian viscosity	U_∞	Free stream velocity
c_p	Specific heat	$\dot{\gamma}$	Magnitude of deformation rate
k	Thermal conductivity	ν	Free stream velocity
B_0	Magnetic factor	ψ	Free stream velocity
		τ_w	Free stream velocity
α_m	Free stream velocity	$(\rho c)_p$	Effective heat capacity of a nanoparticle
v_w	Mass flux velocity	$(\rho c)_f$	Heat capacity of the base fluid
a, b, β	Constants	τ	Parameter defined by the ratio $\frac{(\rho c)_p}{(\rho c)_f}$

Nomenclature			
We	Local Weissenberg number	η	Dimensionless similarity variable
α	Velocity slip parameter	A	Unsteadiness parameter
γ	Curvature factor	Pr	Prandtl number
Ec	Eckert number	*Nb*	Brownian motion
Nt	Thermophoresis diffusion	β^*	Ratio of viscosities
s	Mass flux parameter	δ	Heat sink/source factor
Re	Local Reynolds number	C_f	Skin friction coefficient
Nu	Local Nusselt number	Sh	Local Sherwood number
Sc	Schmidth number	f', θ, ϕ	Dimensionless, velocity, temperature and concentration

List of Tables

List of Figures

distinct γ.

Fig. 12: Variation of $-\theta'(0)$ for distinct α.

Fig. 13 : Variation of $f'(\eta)$ for distinct A.

Fig. 14 and 15: $f'(\eta)$ and $\theta(\eta)$ for distinct M.

Fig. 16 and 17: $f'(\eta)$ and $\theta(\eta)$ for distinct β^*.

Fig. 18 and 19: $\theta(\eta)$ for distinct δ and α.

List of Tables:

Table 1: A comparison of $\mathrm{Re}^{1/2} C_f$ for χ, α and γ when $\beta^* = We = M = A = s = 0$. $(\,)$ – first solution and $[\,]$ – second solution.

α	χ	Ref. [45]		Ref. [30]		Present study	
	$\gamma = 0$						
0	-1.2	(0.932474)	[0.233650]	(0.932468)	[0.233641]	(0.932473)	[0.23365]
-	-1.15	(1.082232)	[0.116702]	(1.082229)	[0.116702]	(1.08223)	[0.116702]
-	0.0	(1.232588)	-	(1.232576)	-	(1.23259)	-
-	0.5	(0.713295)	-	(0.713271)	-	(0.713295)	-
-	2	(-1.887307)	-	(-1.887295)	-	(-1.88731)	-
0.1	-1.2	(1.224941)	[0.182621]	(1.224918)	[0.182621]	(1.22494)	[0.182621]
-	-1.15	(1.306265)	[0.100177]	(1.306234)	[0.100177]	(1.30626)	[0.100177]
-	0.0	(1.134281)	-	(1.134252)	-	(1.13428)	-
-	0.5	(0.632869)	-	(0.632855)	-	(0.632869)	-
-	2	(-1.557650)	-	(-1.557625)	-	(-1.55765)	-
0.2	-1.2	(1.404016)	[0.153829]	(1.404011)	[0.153829]	(-1.40402)	[0.153828]
-	-1.15	(1.442545)	[0.088601]	(1.442528)	[0.088598]	(-1.44255)	[0.0886005]
-	0.0	(1.042585)	-	(1.042563)	-	(1.04258)	-
-	0.5	(0.567044)	-	(0.567033)	-	(0.567044)	-
-	2	(-1.331322)	-	(-1.331303)	-	(-1.33132)	-

Table 2: Values of $\mathrm{Re}^{1/2} C_f$ for distinct curvature parameter γ with $\beta^* = We = M = \alpha = s = 0$ and $\chi = 0.5$.

γ	Omer *et al*. [46]	Hashim and Khan [30]	Present study
0.0	0.7133	0.713283	0.713295
0.2	0.7629	0.762891	0.762907

0.4	0.8101	0.810063	0.810058

List of Figures

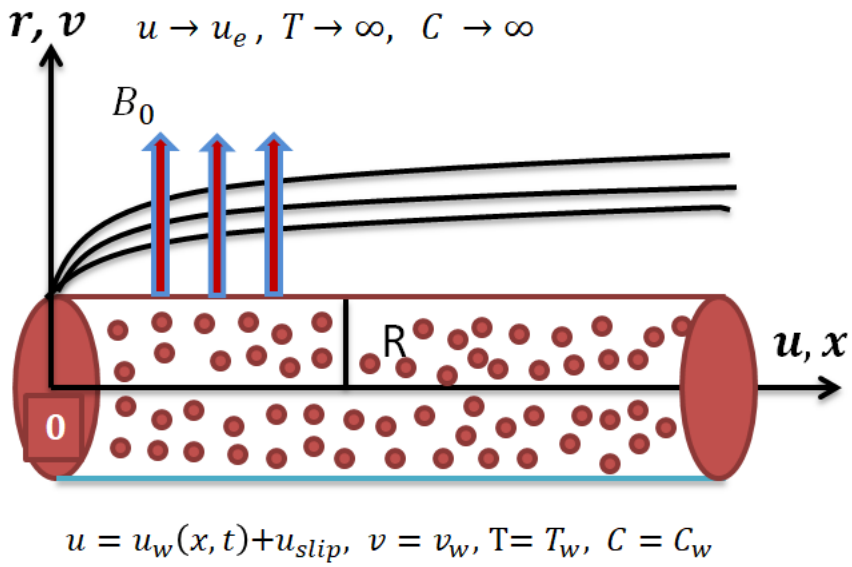

Figure 1

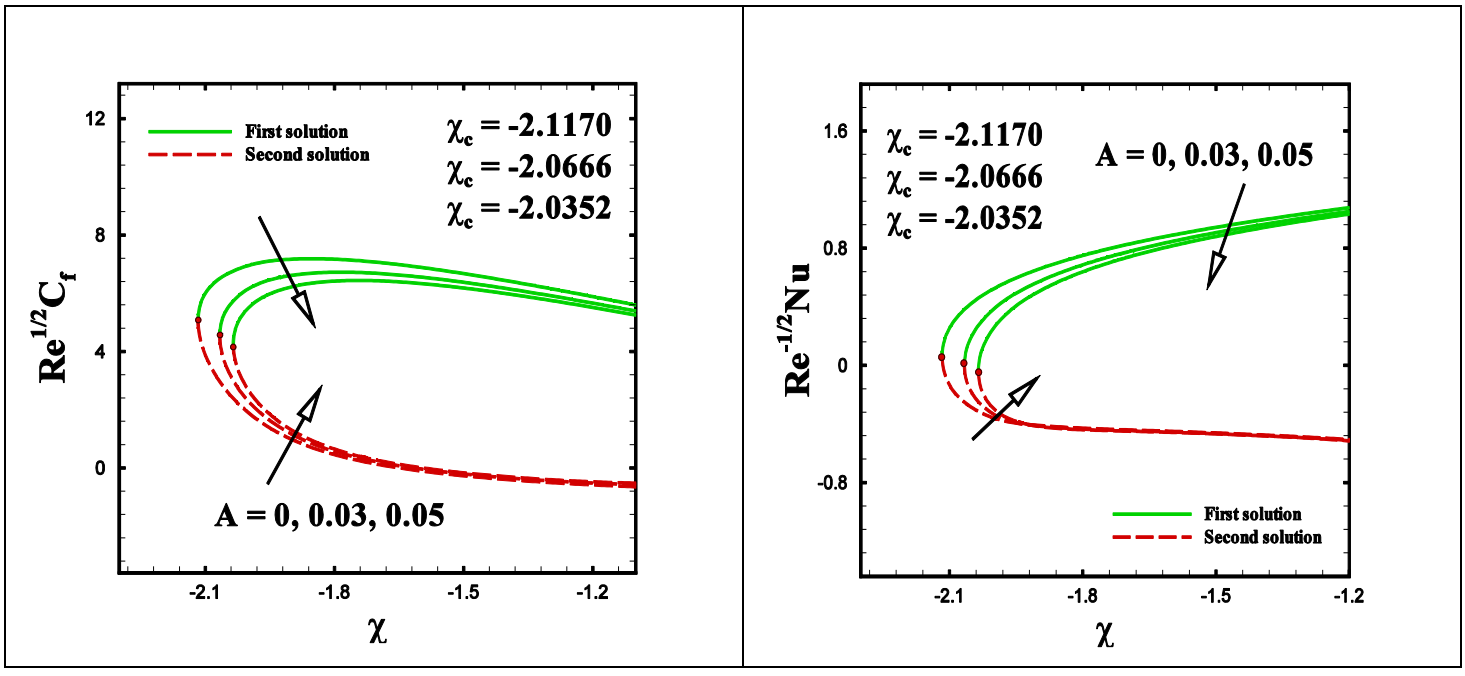

Figure 2 and 3

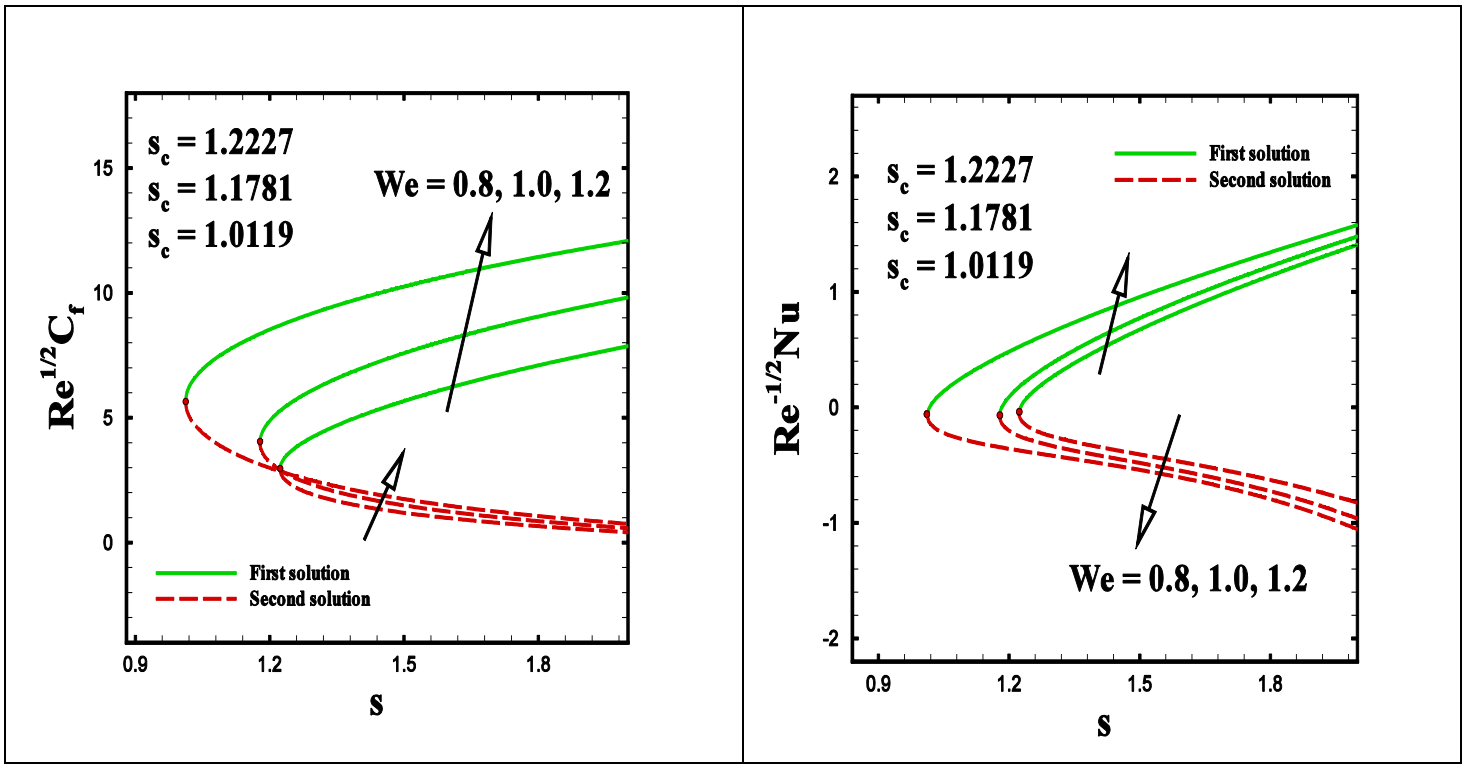

Figure 4 and 5

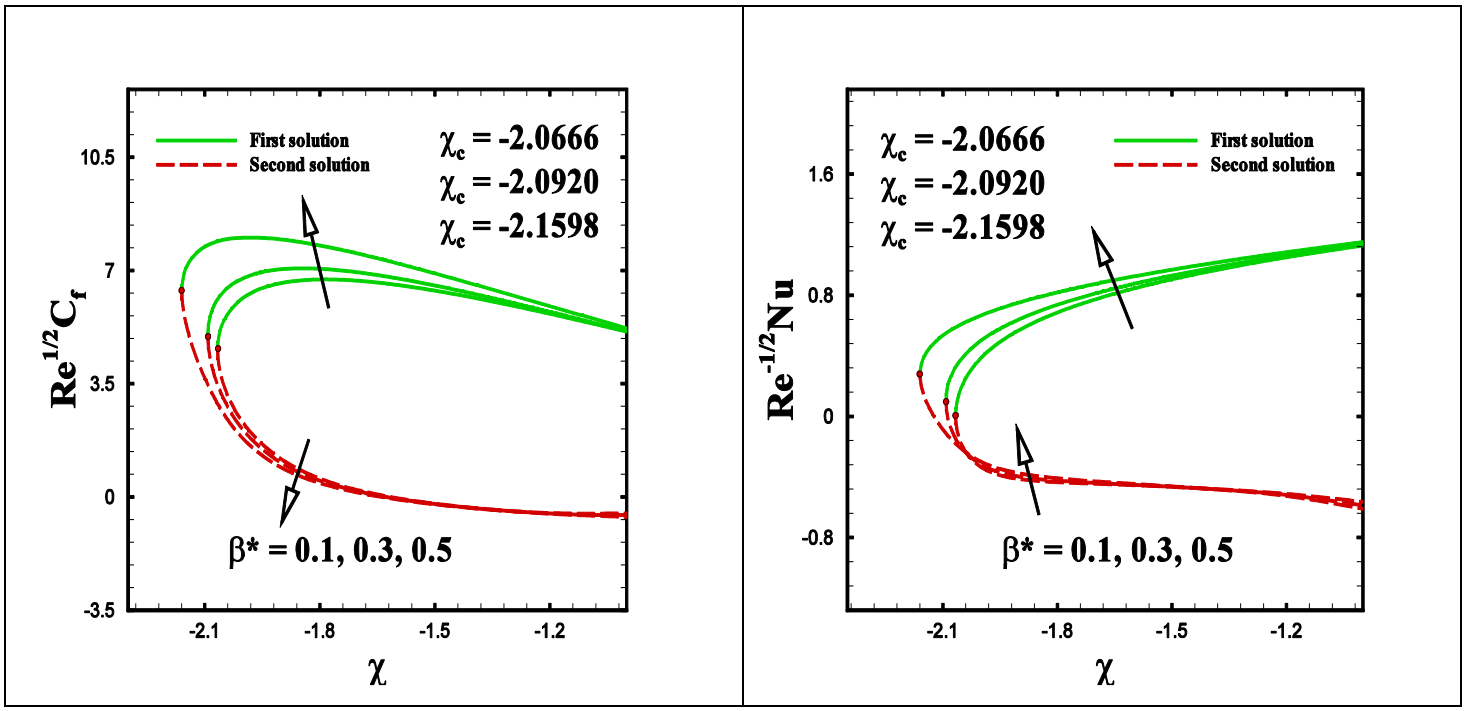

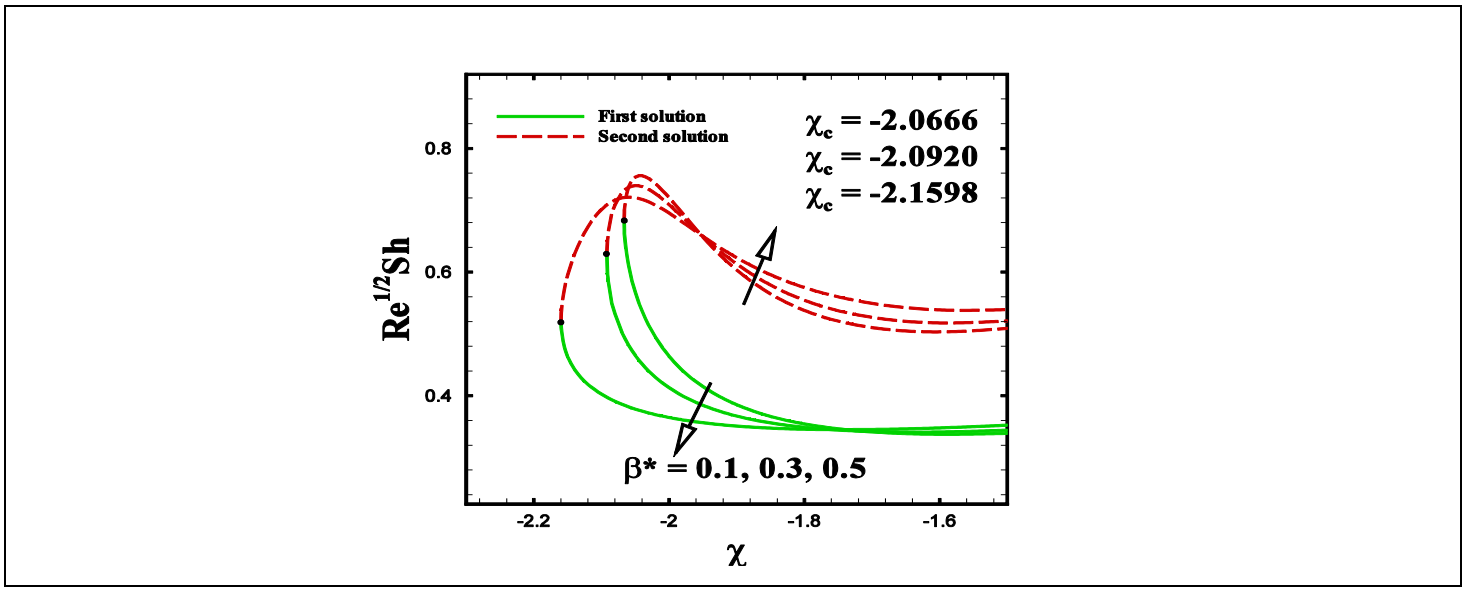
First solution
Second solution
$\chi_c = -2.0666$
$\chi_c = -2.0920$
$\chi_c = -2.1598$
$\beta^* = 0.1, 0.3, 0.5$
$Re^{1/2}Sh$
χ
0.8
0.6
0.4
-2.2
-2
-1.8
-1.6

Figure 8

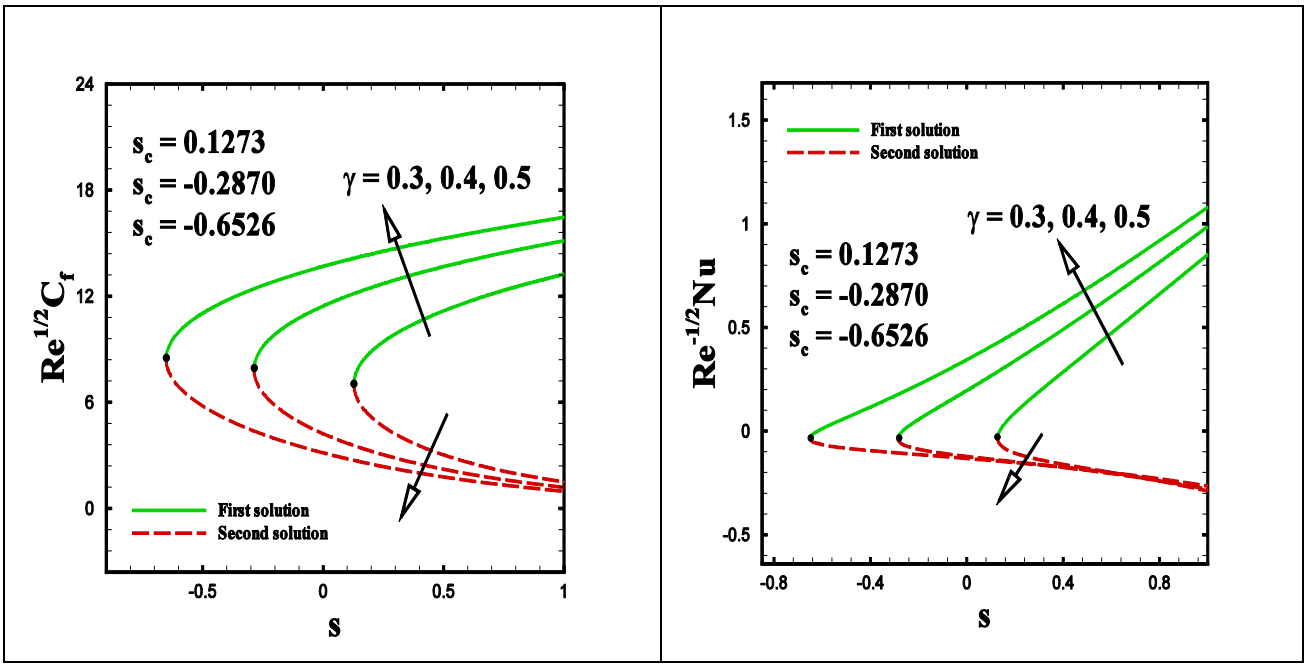
$s_c = 0.1273$
$s_c = -0.2870$
$s_c = -0.6526$
$\gamma = 0.3, 0.4, 0.5$
First solution
Second solution
$Re^{1/2}C_f$
s
24
18
12
6
0
-0.5
0
0.5
1
$Re^{-1/2}Nu$
1.5
1
0.5
0
-0.5
-0.8
-0.4
0.4
0.8

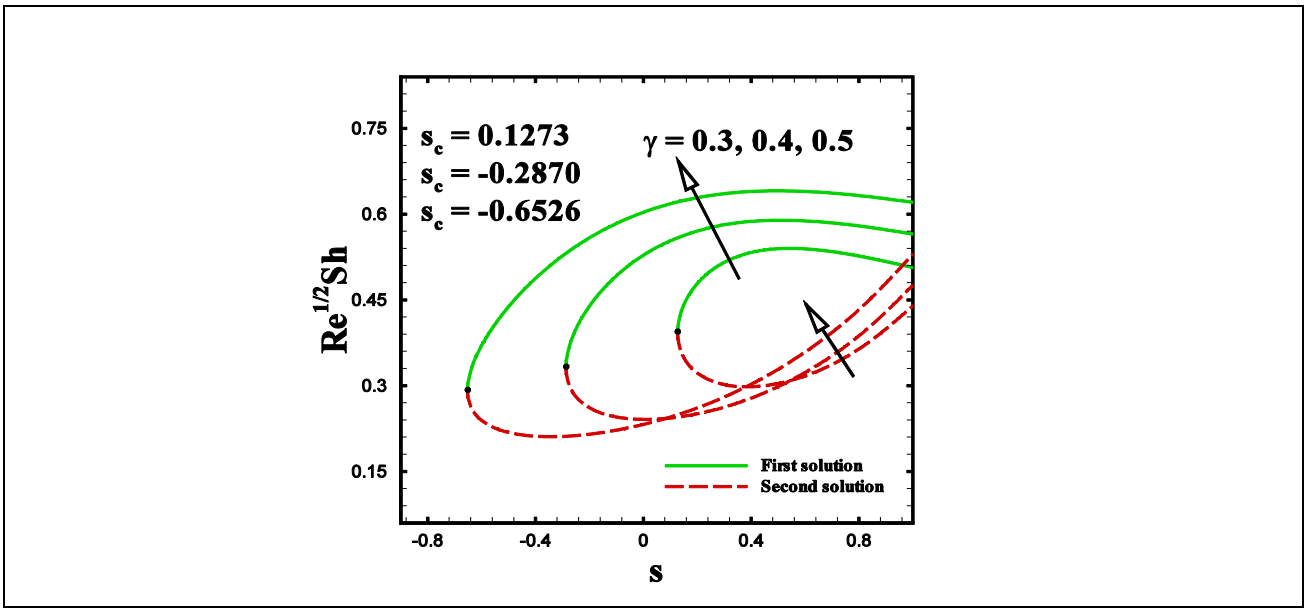

Figure 11

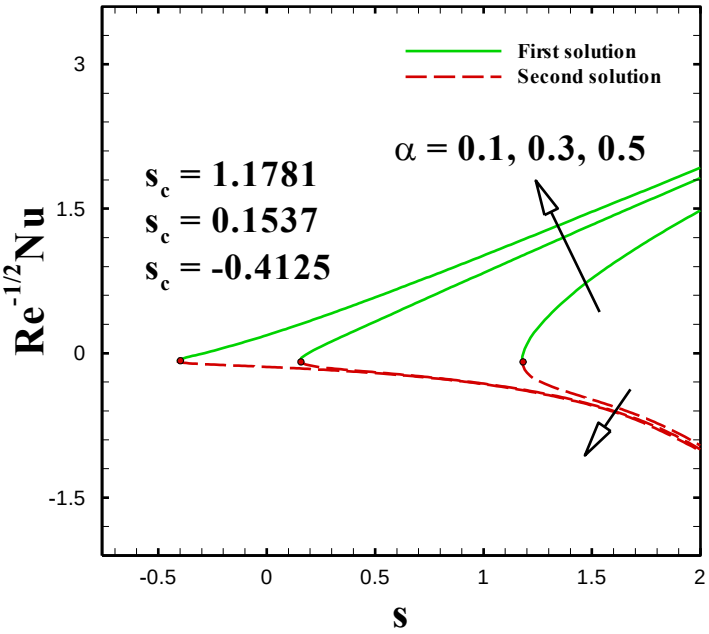

Figure 12

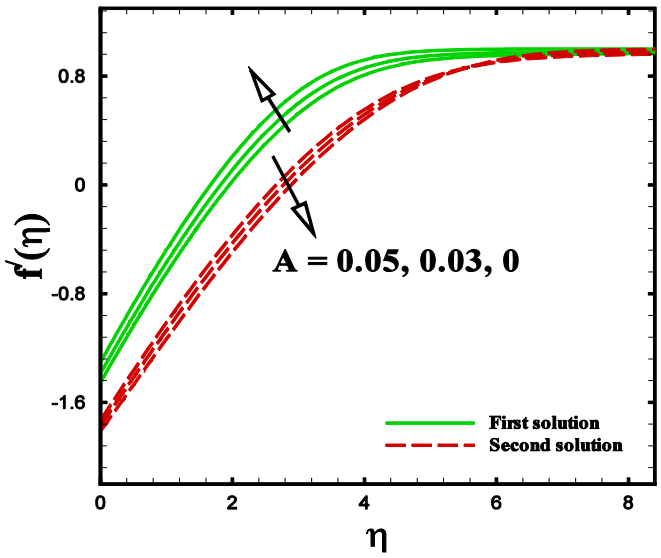

Figure 13

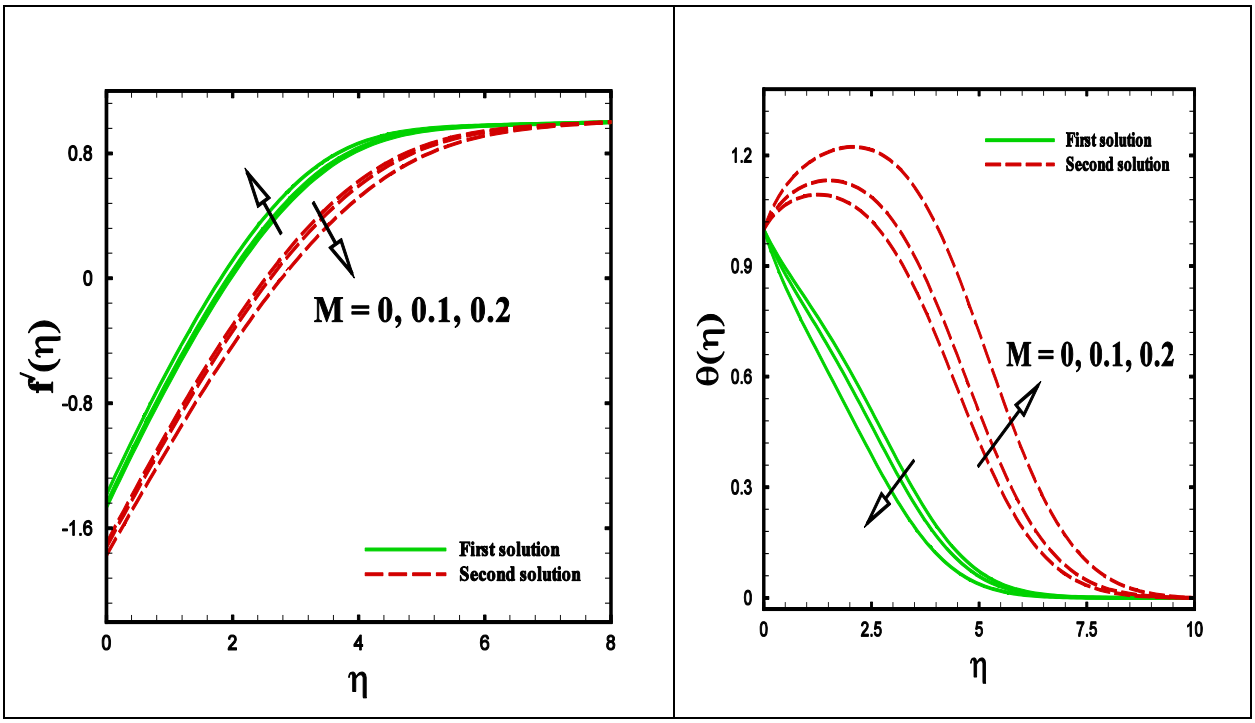

Figure 14 and 15

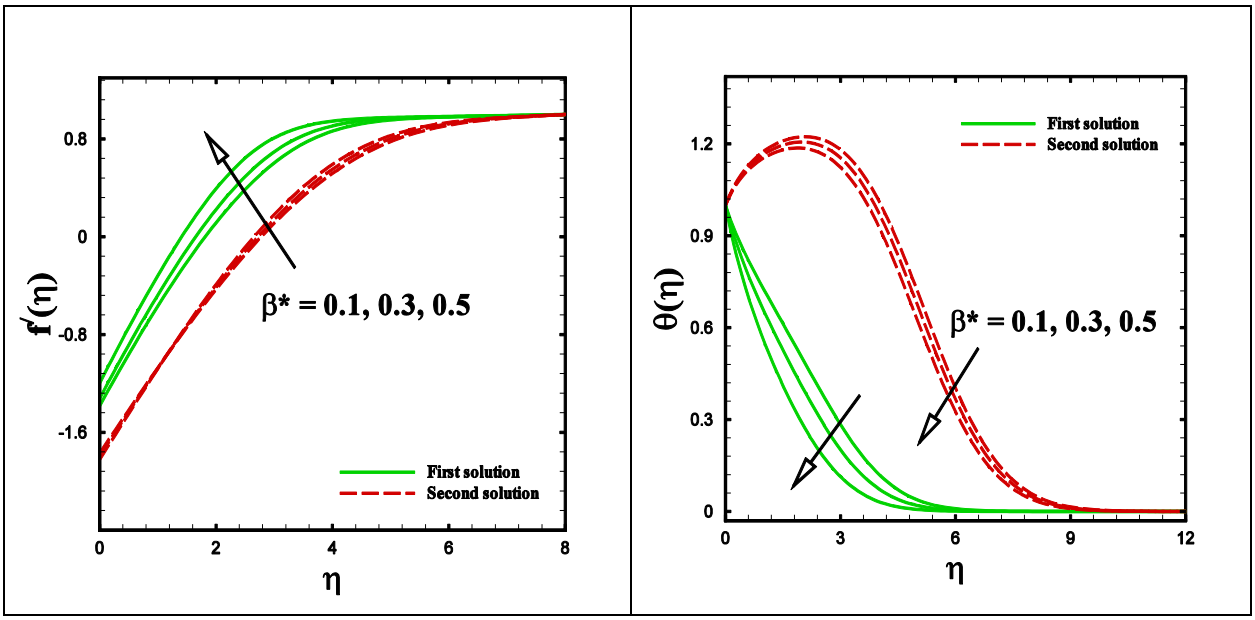

Fig 16 and 17

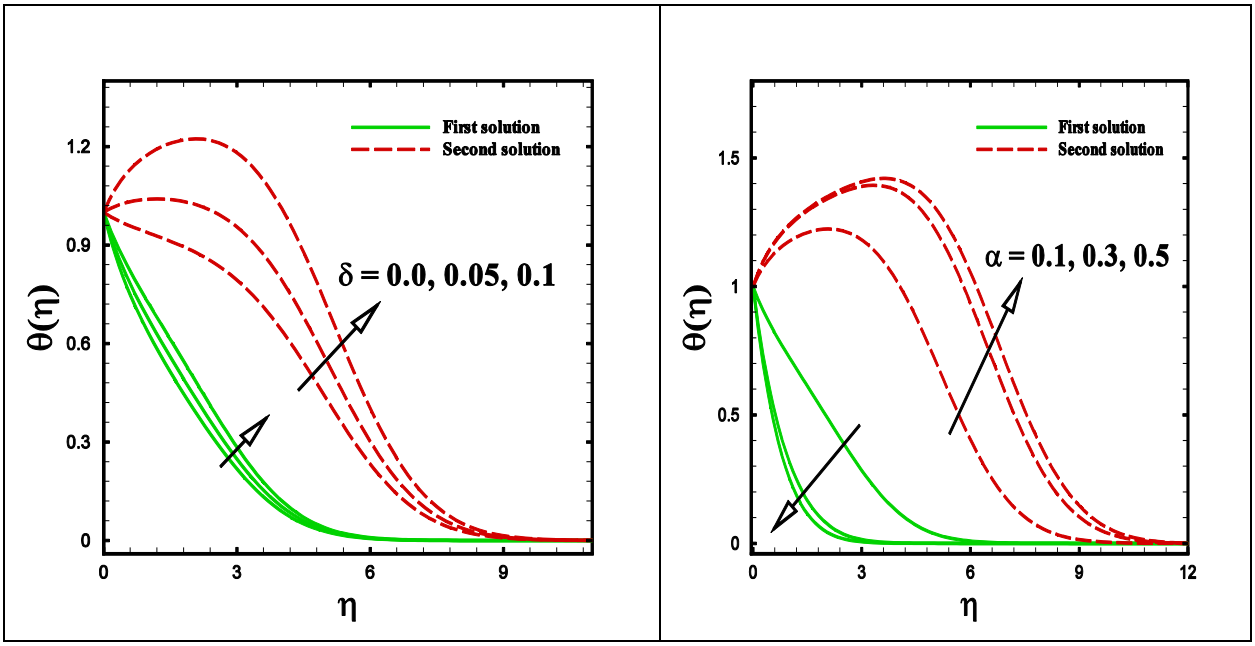

Fig 18 and 19